Multiscale pore-network representation of heterogeneous carbonate rocks

Title: Multi-scale Pore-network Representation of Heterogeneous Carbonate Rocks

Tannaz Pak[1, 2, *], Ian B. Butler[1, 2], Sebastian Geiger[2, 3], Marinus I.J. van Dijke[2, 3], Zeyun Jiang[2, 3], Rodrigo Surmas[2,3,4]

1: School of Geosciences, University of Edinburgh, James Hutton Road, Edinburgh EH9 3FE, UK

2: International Centre for Carbonate Reservoirs, West Mains Road, Edinburgh EH9 3JW, UK

3: Institute of Petroleum Engineering, Heriot-Watt University, Edinburgh EH14 4AS, UK

4: Petrobras Research and Development Centre (Cenpes), Avenida Horácio Macedo, Cidade Universitária, Rio de Janeiro, 21941-915, Brazil

*Current address: School of Science and Engineering, Teesside University, Middlesbrough, TS1 3BA, UK., Corresponding author: Tannaz Pak (t.pak@tees.ac.uk)

Key points:

- This work investigates the multi-scale porosity of a carbonate rock.
- We explore representativeness of multi-scale networks by comparing simulated and laboratory measured capillary-pressure vs saturation curves.
- We present a workflow for selecting number and length scales of networks to generate multi-scale pore-networks.

This article has been accepted for publication and undergone full peer review but has not been through the copyediting, typesetting, pagination and proofreading process which may lead to differences between this version and the Version of Record. Please cite this article as an 'Accepted Article', doi: 10.1002/2016WR018719

Abstract:

A multi-scale network integration approach introduced by *Jiang et al.* [2013] is used to generate a representative pore-network for a carbonate rock with a pore-size distribution across several orders of magnitude. We predict the macroscopic flow parameters of the rock utilising i) 3D images captured by X-ray computed micro-tomography and ii) pore-network flow simulations. To capture the multi-scale pore-size distribution of the rock we imaged four different rock samples at different resolutions and integrated the data to produce a pore-network model that combines information at several length-scales that cannot be recovered from a single tomographic image. A workflow for selection of the number and length-scale of the required input networks for the network integration process, as well as fine tuning the model parameters is presented. Mercury injection capillary-pressure data were used to evaluate independently the multi-scale networks. We explore single-scale, two-scale, and three-scale network models and discuss their representativeness by comparing simulated capillary-pressure versus saturation curves with laboratory measurements. We demonstrate that for carbonate rocks with wide pore-size distributions, it may be required to integrate networks extracted from two or three discrete tomographic data sets in order to simulate macroscopic flow parameters.

1. Introduction

Pore-scale fluid flow simulation is a useful tool for calculation of the macroscopic transport properties of porous media, specifically for homogeneous systems [*Meakin and Tartakovsky*, 2009; *Joekar-Niasar and Hassanizadeh*, 2012; *Blunt et al.*, 2013; *Wildenschild and Sheppard*, 2013]. For complex porous material realistic representation of the pore structure is essential for successful simulations but has proven to be challenging. High-resolution X-ray computed micro-tomography (μCT) imaging allows detailed study of porous media in 3D (reviews by *Wildenschild and Sheppard* [2013], *Fusseis et al.* [2014], and *Bultreys et al.* [2016]). Reliable application of this technique requires sufficient image quality to allow discrimination of the important features of the sample. Pore-network models (PNM) extracted from binarised μCT images (see review by *Dong* [2007]) are simple representations of pore

structures to simulate flow at a reduced computational cost. Although appealing, PNM predictions often do not agree well with the corresponding laboratory measurements, specifically for complex pore systems such as carbonate rocks [*Sorbie and Skauge*, 2012]. The trade-off between the sample size and μCT image resolution means that a single μCT volume may not capture the details of a multi-scale pore structure [*Hebert et al.*, 2014]. Capturing a representative image of heterogeneous samples with pore-size distribution (PSD) spanning several orders of magnitude is an outstanding challenge with existing μCT instrumentation. A representative elementary volume (REV) is required that is the smallest sample to which measured properties of the bulk sample can be assigned [*Bear*, 1972]. Generating two-scale PNM that are representative of complex pore systems has been studied by *Biswal et al.* [2007]; *Biswal et al.* [2009] and *Ghous et al.* [2008], and more recently by *Prodanović et al.* [2015], *Mehmani and Prodanović* [2014], and *Bultreys et al.* [2015].

Jiang et al. [2013] introduced a network integration method to generate PNMs of arbitrarily large volumes that can incorporate multi-scale pore systems extracted [*Jiang et al.*, 2007] from images captured at different resolutions. A detailed PNM extracted from a high resolution μCT volume (fine-network) is combined with a network extracted from a coarse resolution volume (coarse-network). For details of how the nodes/bonds of the differently scaled models are interconnected see *Jiang et al.* [2013]. The domain of the fine-network is smaller than that of the coarse-network, hence a larger network that is statistically equivalent to the fine-network is generated and then integrated into the coarse-network. The generated multi-scale networks can be heavier than the original fine-network, with an adverse effect on the computational cost of fluid flow simulations. To address this *Jiang et al.* [2013], reduced the number of fine-network elements by a fraction (f_F) such that $0<f_F\leq1$. It is also possible to scale the size of the domain of the two-scale network (nesting-domain) with respect to that of

the original coarse image using a scaling factor (δ) that is arbitrary but is restricted by the available computational power for flow simulations.

We investigate generation of a representative PNM for a dolomite using *Jiang et al.* [2013]'s approach and a quasi-static pore-network flow simulator [*Ryazanov et al.* [2009]. We evaluate *Jiang et al.* [2013]'s approach by comparing simulated $P_c(S)$ curves with those measured experimentally using mercury injection capillary-pressure (MICP) tests. A workflow is proposed for multi-scale network generation to address (i) the choice of sample size and, hence, image resolution, and (ii) the tuning of model parameters to reproduce the laboratory $P_c(S)$ curves.

2. Imaging and Mercury Porosimetry

A sucrosic dolomite (Silurian Dolomite (SD), Thornton formation, Chicago, Illinois, US) with pore sizes spanning 3 orders of magnitude was used (Figure 1). Laboratory measurements of a 38mm diameter core displayed porosity and permeability of 17% and ~50mD, respectively (Figure 1b).

We imaged, using μCT, four samples of diameter D=2, 5, 25 and 38mm, at resolutions of 2.3, 12, 21 and 32.8μm, respectively (Figure 1b). Both the image voxel sizes and the corrected image resolutions are reported in Table 1, the correction accounts for the unsharpness caused by the X-ray source spot size [*Feser et al.*, 2008]. The values presented throughout the rest of the manuscript are the corrected image resolution values. As currently worded, this is still a bit unclear. Methods are detailed in the SI and *Pak et al.* [2013]. Sizes were selected because 38mm is a standard petrophysical plug, 25mm is the largest sample the MICP could analyse, and 5mm and 2mm provide details of the finer porosity. Figure 1c displays the PSD derived from these four data volumes (Figure 1b) using a sphere fitting method [*Jiang et al.*, 2007]. Each volume has captured only a portion of the PSD. In SD recrystallization to dolomite has produced a structure in which the pores are lined by the apices and edges of dolomite rhombs

with well sorted crystals sizes. Microscope images (Figure S1.) show that smaller pores are formed in between a few crystals, are uniformly present throughout the sample, suggesting little or no spatial correlation of the micro-porosity. Hence, we uniformly integrate the fine-network in the entire nesting-domain.

MICP measurement was performed on three 25 mm diameter SD core plugs imaged at resolution 21μm (Figure S2). MICP provides $P_c(S)$ curves from which pore-throat size distribution can be extracted [*Ritter and Drake*, 1945]. The MICP-based porosity for these samples is 18.03, 16.03 and 18.1%. The image-based porosities at this resolution are 8.05, 6.03 and 8.12%, respectively, hence the 21μm represent a coarse-scale resolution.

3. Multi-scale PNM Reconstruction

We explore representing the SD pore structure using multi-scale networks to incorporate features extracted from the four μCT volumes shown in Figure 1b. For 3D renderings of these networks see Figure S3. The physical size of these networks can be found from the image dimensions and voxel resolutions (Table 1). The two coarse-scale networks are globally disconnected while the fine-scale networks are connected with simulated absolute permeability k_{abs}>0mD. The total (and connected) porosity shows an increasing trend with resolution enhancement, as does the calculated permeability. The two fine-networks display calculated permeability values higher than the laboratory measurement i.e. 50 mD. The small samples do not contain a REV and the calculated permeability values reflect the local connectivity of the pore system at these scales. However, even for the 2.3μm resolution network about 11% of the pore volume is disconnected, reflecting that the resolution is insufficient to capture the smallest pore-throats, or that isolated pores exist in the sample.

3.1. Two-scale PNMs

Six possible combinations for generating two-scale networks are 32.8-21μm, 32.8-12μm, 32.8-2.3μm, 21-12μm, 21-2.3μm, and 12-2.3μm, referring to image resolution. Essentially, we need (i) a sufficiently large coarse-network that represents the largest pores, (ii) a fine-network with sufficient resolution that captures the smaller pores, and (iii) a sufficient overlap of the PSD of the two networks to ensure representation of the intermediate-size pores. Hence, 12-2.3μm and 32.8-21μm combinations are not acceptable. In what follows other combination are discussed.

3.1.1. Combination of 21 and 2.3μm PNMs

Figure 2a shows ten networks extracted from sub-domains (δ=0.1-1) of the 21μm coarse-network. At δ=0.4 the domain is sufficiently large to accommodate a cluster of large pores,

hence the network porosity displays a sharp increase, Figure 2b. At δ=0.5 the domain accommodates a connected cluster of pores, therefore, k_{abs}>0. However, as the sub-domain grows (δ>0.5) the networks become again disconnected, suggesting that only a locally connected cluster is captured at δ=0.5 which is not representative of the connectivity of larger pores at this scale.

Figure 2c displays the sensitivity of these two-scale networks to f_F. Porosity increases linearly with the inclusion of increasing fractions of the fine-network, while the permeability starts to converge for f_F>0.05. Thus even a reduced version of a fine-network can provide the required connectivity to two-scale network.

The calculated porosity and permeability display convergence at δ>0.6 (i.e. total porosity ~6% and k_{abs}=0). Figure 2d, however, shows that the $P_c(S)$ curves, calculated using these two-scale PNMs (f_F=0.01, 0.6<δ<1), do not converge. The curves display jumps at different saturations depending on the nesting-domain size. Examination of Figure 2a reveals that the coarse-network contains two connected clusters of elements (pores and nodes) that are disconnected from each other. Network integration provides connectivity between these clusters through elements of the fine-network. Cluster 1 is connected to the inlet and can be invaded by the injected phase directly. Cluster 2 is only accessible through cluster 1 using the fine-network connections. The jump occurs at saturation S^* that is equal to the ratio of the volume of cluster 1 to the total volume of the connected pore space.

As δ increases, cluster 2 grows more significantly compared to cluster 1, hence S^*approaches 0.8. Hence, the selected domain from the 21μm resolution image does not contain a REV. However, the MICP core plugs were approximately 60% larger than the box selected for pore-network simulations, and the MICP-driven $P_c(S)$ curves for three 25mm diameter SD plugs are very close (Figure S2a), this suggests that the MICP plugs themselves are representative for this rock.

3.1.2. Combination of 32.8 and 2.3μm PNMs

For this combination the two-scale network porosity converges for δ>0.6 (Figure 3a) while k_{abs}=0 for all sub-domains. Further, the simulated $P_c(S)$ curves for this combination (f_F=0.01) also converge for δ>0.6 (Figure 3b). This indicates that sub-domains of the 38.2μm image with δ>0.6 contain a REV of SD. The $P_c(S)$ curves, however, show a jump at S_{air}~0.8 causing an overestimation of the experimental capillary-pressure values for S_{air}<0.8. The PSD of the 2.3μm network (Figure 1b) shows a peak at ~6μm, while pores larger than 10μm display less than 20% probability (i.e. volume fraction). Since the coarse-network is globally disconnected, the two-scale networks are connected only through fine-network elements. The initial displacement (S_{air}>0.8) corresponds to the pores accessible from the inlet. At S_{air}~0.8 the pressure needs to increase sufficiently before elements from the fine-network can be invaded. For the converged set of $P_c(S)$ curves, on Figure 3b, the f_F is equal to 0.01. Including a larger f_F suppresses the jump in the capillary-pressure curve but does not totally remove it. The $P_c(S)$ curve for the δ=0.6 and f_F=0.04 network shows a small jump at S_{air}=0.8 from ~21kP to ~47kP corresponding to invasion of pore-throats with radius of 40μm to 16μm. However, this size range is insufficiently represented in both 32.8 and 2.3μm networks. In particular, a small f_F makes a reduced network less representative of the two ends of the PSD. In practice, the difference in the domain sizes of the coarse and fine-networks causes higher f_F values to make the two-scale network substantially more computationally expensive.

3.1.3. Combination of 32.8 and 12μm PNMs

For this combination the calculated $P_c(S)$ curves show a good match with the laboratory measurements at S_{air}>0.04 (Figure 4). However, the simulations stop at capillary-pressure values around 276kP, due to fine-network resolution limitations. Using a higher resolution

fine-network may not provide significant additional connectivity, but may prove essential for calculation of saturation values.

3.2.Three-scale PNMs

We have demonstrated that a finer length-scale needs to be integrated into the 32.8–12μm combination, or an intermediate length-scale must be added to the 32.8–2.3μm combination. To integrate three PNMs of different length-scales first the two smaller networks are integrated into a two-scale network that is subsequently integrated into the largest scale network. This involves selecting two sets of δ and f_F. As the number of length-scales increases, sensitivity analysis on the effect of δ and f_F becomes increasingly time consuming. Figure 5 compares the closest simulated three-scale network $P_c(S)$ curve with the laboratory measurement. This three-scale PNM is generated by integration of the 2.3 and 12μm networks (δ=1, f_F=0.004) followed by integration of that network with the 32.8μm network (δ=0.7, f_F=0.006). The nesting-domain sizes for the 2.3 and 12μm networks are close, hence selecting δ=1 is feasible. To keep the three-scale network computationally manageable while ensuring representativity, we selected δ=0.7 for the second step.

Sensitivity analysis was performed on the value of f_F within the range of 0.001 to 0.1 for the first step and 0.001 to 0.006 for the second step. The calculated $P_c(S)$ curves show that keeping the first f_F value at 0.004 enables the inclusion of a sufficient number of elements from the 2.3μm network for simulations to predict the higher capillary-pressures while eliminating artificial jumps in capillary-pressure.

We analysed the goodness of fit for the $P_c(S)$ curves for the single (at 2.3μm and 12μm), two-scale, and three-scale PNMs using the Chi-squared measure. Single-scale networks yield the poorest capillary-pressure predictions while the three-scale network and the two-scale (32.8-12μm) show only minor deviations from the laboratory measurements (Figure 5). Chi-squared for the 32.8-12μm network is marginally better that of the 32.8-12-2.3μm network,

since the Chi-squared test only compares model predictions against the laboratory measurements, but does not capture that the model does not predict capillary-pressures at low saturations for the 32.8-12µm combination.

Although the calculated absolute permeability values (Table 2) do not accurately match the experimental observation (50mD), the calculated values are close and within the same order of magnitude. The deviation could stem from (i) the fact that the simulations are conducted on a subsection of the acquired µCT images, (ii) errors introduced in noise filtering and subsequent segmentation steps, and (iii) image properties, in particular, the partial volume effect. This can cause features (e.g. pore-throats) smaller than one voxel to appear as large as a voxel in the segmented images. Larger pore-throats display less resistance to the flow and hence a higher absolute permeability is calculated.

No laboratory *kr(S)* measurements were available, hence simulated *kr(S)* curves for single and multi-scale PNMs are compared in SI. In summary, we show that the parameters involved in the network integration, as well as the number and resolution of the input single-scale networks can have a substantial impact on the shape of the *kr(S)* curves calculated based on the multi-scale PNMs. Future studies could aim to compare the calculated *kr(S)* curves with laboratory measurements to establish the effect of network integration on predicting *kr(S)* curves.

4. Multi-scale Network Generation Workflow

Figure 6 is a practical guide for selection of length-scales for generating a multi-scale PNM from µCT data and is additionally informed by thin-section imaging and MICP techniques. This information assists sample size selection, the choice of length-scales, and resolutions for multi-scale network generation.

5. Summary and Conclusions

A network integration approach introduced by *Jiang et al.* [2013] is used to generate representative models for a dolomite with multi-scale porosity. PNMs extracted from μCT images acquired at different length-scales are integrated into single multi-scale PNMs incorporating all the porosity features that exist in the rock. The main contribution of this paper is to present a workflow for effective selection of appropriate length-scales for generation of the multi-scale network. The choice of images to be combined is informed by MICP throat-size distributions. Additionally, there are two free parameters (δ and f_F) in the model. The integrated networks are used to reproduce $P_c(S)$ curves, evaluated against MICP laboratory measurements. We demonstrate that $P_c(S)$ curves calculated based on the two-scale and three-scale PNMs provide significantly closer comparisons to the laboratory measurements compared to a single-scale network model. Future studies need to validate calculated *kr(S)* curves against experimental measurements to optimise multi-scale network generation for predictions of multiphase fluid behaviour.

Acknowledgement:

We would like to thank Petrobras and BG Group for their sponsorship of the ICCR programme and the permission to publish this work from the project SatuTrack. We thank Petrobras Research Centre for the mercury injection capillary-pressure tests, Mike Hall for preparing the thin-sections, and the Centre of Environmental Scanning Microscopy at Heriot-Watt University. All data for this paper is properly cited and referred to in the reference list. Simulations were carried out with the PAT software developed at Heriot-Watt University. Input data and software used in this paper can be obtained from the authors upon request.

References:

Bear, J. (1972), *Dynamics of Fluids in Porous Media*, Elsevier, New York.
Biswal, B., P. Øren, R. Held, S. Bakke, and R. Hilfer (2007), Stochastic multiscale model for carbonate rocks, *Phys. Rev. E: Stat., Nonlinear, Soft Matter Phys.*, *75*(6), 061303.
Biswal, B., P. Øren, R. J. Held, S. Bakke, and R. Hilfer (2009), Modeling of multiscale porous media, *Image Analysis and Stereology*, *28*, 23-34.
Blunt, M. J., B. Bijeljic, H. Dong, O. Gharbi, S. Iglauer, P. Mostaghimi, A. Paluszny, and C. Pentland (2013), Pore-scale imaging and modelling, *Adv. Water Resour.*, *51*, 197-216.
Bultreys, T., L. Van Hoorebeke, and V. Cnudde (2015), Multi-scale, micro-computed tomography-based pore network models to simulate drainage in heterogeneous rocks, *Adv. Water Resour.*, *78*, 36-49.
Bultreys, T., W. De Boever, and V. Cnudde (2016), Imaging and image-based fluid transport modeling at the pore scale in geological materials: A practical introduction to the current state-of-the-art, *Earth-Science Reviews*, *155*, 93-128.
Dong, H. (2007), *Micro-CT imaging and pore network extraction*.
Feser, M., J. Gelb, H. Chang, H. Cui, F. Duewer, S. Lau, A. Tkachuk, and W. Yun (2008), Sub-micron resolution CT for failure analysis and process development, *Measurement science and technology*, *19*(9), 094001.
Fusseis, F., X. Xiao, C. Schrank, and F. De Carlo (2014), A brief guide to synchrotron radiation-based microtomography in (structural) geology and rock mechanics, *Journal of Structural Geology*, *65*, 1-16.
Ghous, A., et al. (2008), 3D Imaging of Reservoir Core at Multiple Scales; Correlations to Petrophysical Properties and Pore Scale Fluid Distributions, edited, International Petroleum Technology Conference.
Hebert, V., C. Garing, L. Luquot, P. A. Pezard, and P. Gouze (2014), Multi-scale X-ray tomography analysis of carbonate porosity, *Fundamental Controls on Fluid Flow in Carbonates: Current Workflows to Emerging Technologies. Geological Society, London, Special Publications*, *406*.
Jiang, Z., M. Dijke, K. Sorbie, and G. Couples (2013), Representation of multiscale heterogeneity via multiscale pore networks, *Water Resour. Res.*, *49*(9), 5437-5449.
Jiang, Z., K. Wu, G. Couples, M. Van Dijke, K. Sorbie, and J. Ma (2007), Efficient extraction of networks from three-dimensional porous media, *Water Resour. Res.*, *43*(12).
Joekar-Niasar, V., and S. Hassanizadeh (2012), Analysis of fundamentals of two-phase flow in porous media using dynamic pore-network models: A review, *Critical Reviews in Environmental Science and Technology*, *42*(18), 1895-1976.
Meakin, P., and A. M. Tartakovsky (2009), Modeling and simulation of pore-scale multiphase fluid flow and reactive transport in fractured and porous media, *Rev. Geophys.*, *47*(3), RG3002.
Mehmani, A., and M. Prodanović (2014), The effect of microporosity on transport properties in porous media, *Adv. Water Resour.*, *63*, 104-119.
Pak, T., S. Geiger, Z. Jiang, K. S. Sorbie, S. Elphick, M. I. J. van Dijke, and I. Butler (2013), Pore-Scale Visualisation of Two-Phase Fluid Displacement Processes in a Carbonate Rock using X-ray micro-Tomography Technique, in *SPE Reservoir Characterization and Simulation Conference and Exhibition*, edited, Society of Petroleum Engineers, Abu Dhabi, UAE.
Prodanović, M., A. Mehmani, and A. P. Sheppard (2015), Imaged-based multiscale network modelling of microporosity in carbonates, *Geological Society, London, Special Publications*, *406*(1), 95-113.
Ritter, H., and L. Drake (1945), Pressure porosimeter and determination of complete macropore-size distributions. Pressure porosimeter and determination of complete

macropore-size distributions, *Industrial & Engineering Chemistry Analytical Edition*, *17*(12), 782-786.
Ryazanov, A. V., M. I. J. van Dijke, and K. S. Sorbie (2009), Two-Phase Pore-Network Modelling: Existence of Oil Layers During Water Invasion, *Transp. Porous Media*, *80*(1), 79-99.
Sorbie, K., and A. Skauge (2012), Can network modeling predict two-phase flow functions?, *Petrophysics*, *53*(06), 401-409.
Wildenschild, D., and A. P. Sheppard (2013), X-ray imaging and analysis techniques for quantifying pore-scale structure and processes in subsurface porous medium systems, *Adv. Water Resour.*, *51*(0), 217-246.

Nomenclature Table:

S	saturation
S^*	the saturation at which the jump occurs
S_{air}	air saturation
$\boldsymbol{f_F}$	Fraction of fine network
$\boldsymbol{\delta}$	Nesting-domain fraction
$P_c(S)$	relative permeability
$k_r(S)$	relative permeability
$krnw(S)$	non-wetting phase relative permeability
$krw(S)$	wetting phase relative permeability
k_{abs}	absolute permeability
r	radius
χ^2	Chi-squared

Tables:

Table 1: Network parameters for PNM shown in Figure S3.

Image Resolution (µm), corrected for spot size	Voxel Size (µm)	Domain Dimensions (voxels)	Number of Nodes	Number of Bonds	Connected Porosity %	Total imaged Porosity %	k_{abs} (mD)

32.8	32	881×901×901	10318	12736	0	3.52	0
21	21	821×860×720	19897	24093	0	6.03	0
12	5	500×500×500	3418	4127	6.15	9.23	75.63
2.3	2	570×450×380	1733	2089	12.72	14.32	99.75

Table 2: Network parameters for multi-scale PNMs

Image Resolution (μm)	Number of Nodes	Number of Bonds	Connected Porosity %	Total Porosity %	k_{abs} (mD)	Average coordination number
32.8-12-2.3	13956	22954	3.81	3.96	128.14	3.44
32.8-2.3	439131	534791	3.31	3.36	178.02	3.02
32.8-12	76916	100743	4.28	4.43	90.55	2.94

Figure Captions:

Figure 1: (a) Backscattered SEM image of a polished thin-section of SD in three different magnifications, acquired at SEM facility at Heriot-Watt University (resolution ~0.7μm). The left hand side image represents a tessellated image constructed from 400 fields of view stitched together, (b) Four μCT images of SD rock samples (D=2, 5, 25 and 38mm) captured at respective resolutions of 2.3, 12, 21 and 32.8μm. The scanned samples were not generated sequentially by cutting the same core, (c) PSD derived from the four images shown in (b) using a sphere fitting method [Jiang et al., 2007].

Figure 2: (a) Networks extracted from ten sub-domains with δ ranging from 0.1 to 1 for the coarse-network (resolution 21μm), blue colour shows connected pink is globally disconnected elements, (b) Static properties of the sub-domain networks shown in (a), the blue box corresponds to the jump in the total porosity captured for δ=0.4 while the red box shows the locally connected cluster captured in the sub-domain with δ=0.5, (c) Effect of fraction of fine-network (f_F) on porosity and permeability of two-scale networks with δ=0.7 (see 3D renderings in Figure S4), and (d) Effect of nesting-domain size on the two-scale (21 and 2.3μm, f_F=0.01) $P_c(S)$ curves in comparison with laboratory measurements.

Figure 3: (a) The porosity of the sub-domains of the 32.8μm network as a function of the domain fraction, (b) The $P_c(S)$ curves for the combined 32.8 – 2.3μm networks compared with the MICP laboratory measurements. The 32.8μm network becomes sufficiently representative for δ>0.6 displaying converged porosity and $P_c(S)$ curves. δ: Nesting-domain fraction, f_F: Fraction of fine-network.

Figure 4: The $P_c(S)$ curves for the two-scale 32.8–12µm (δ=0.7) network for various f_F. The model predictions show a good fit to the experimental data, however, the model does not predict the higher pressure end of the curve.

Figure 5: The $P_c(S)$ curves for the three-scale network compared with the laboratory data, two-scale and single-scale simulations. The plot also shows the Chi-squared (χ^2) measure for these networks. The three-scale network model displays the best fit to the MICP data.

Figure 6: Multi-scale network generation workflow and tuning.

Figure 1. Figure

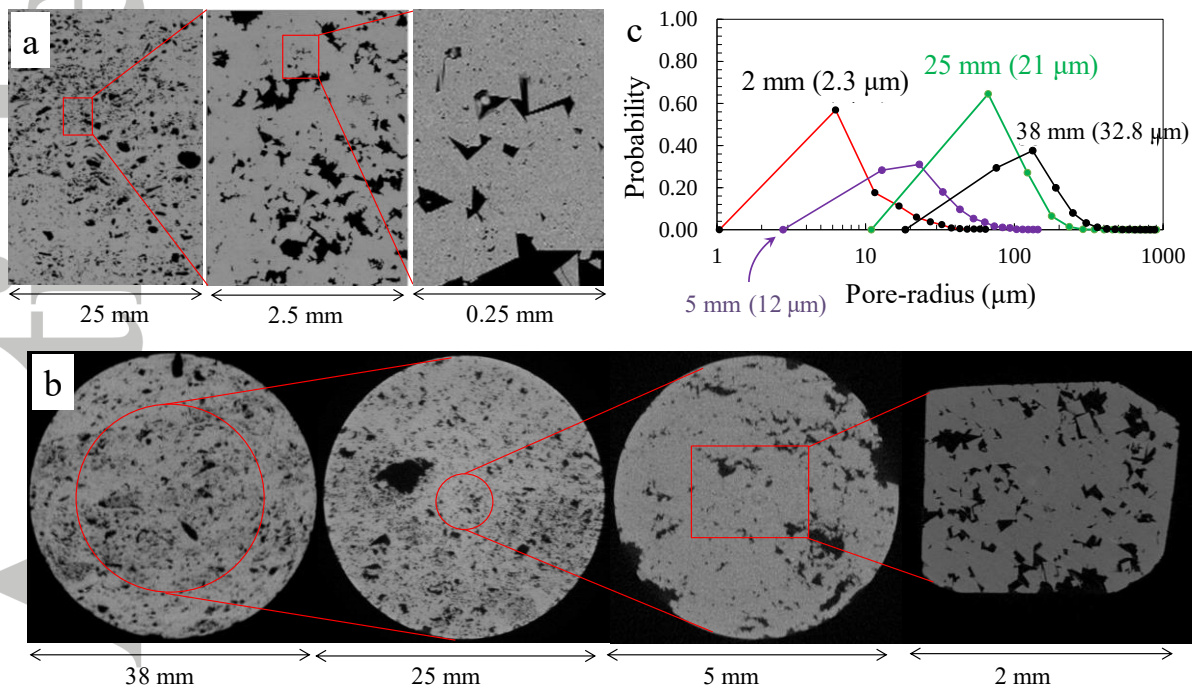

Figure 2. Figure

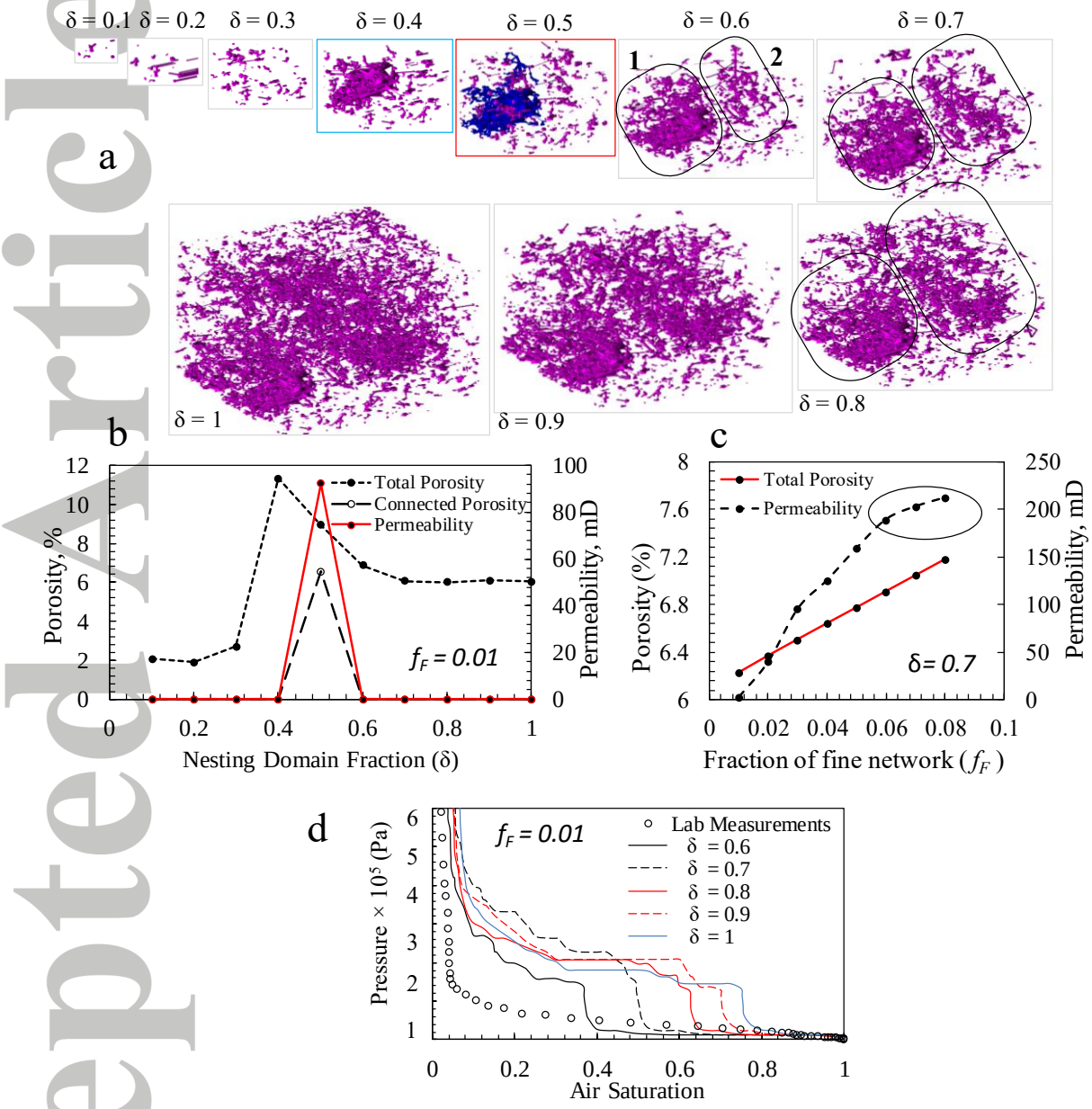

Figure 3. Figure

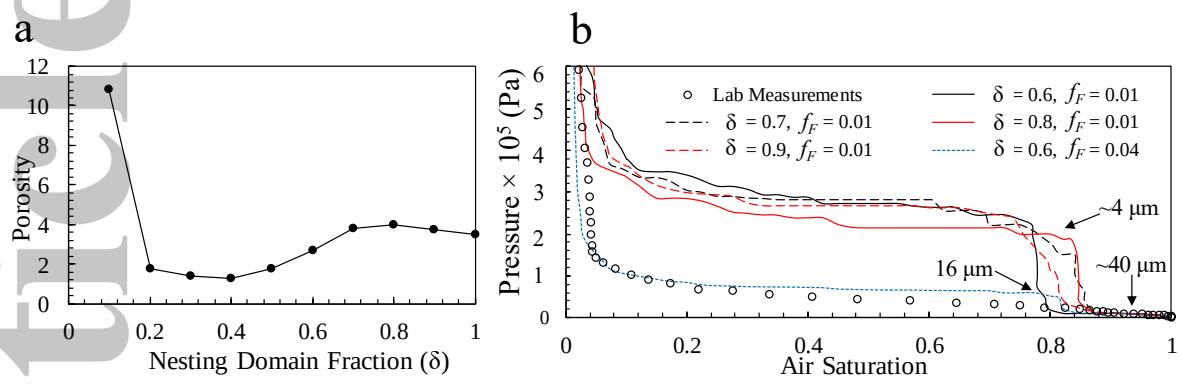

Figure 4. Figure

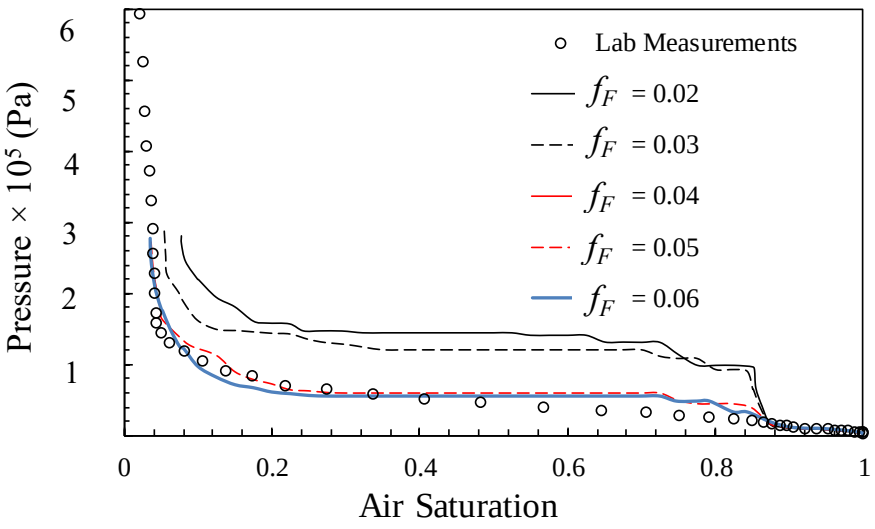

Figure 5. Figure

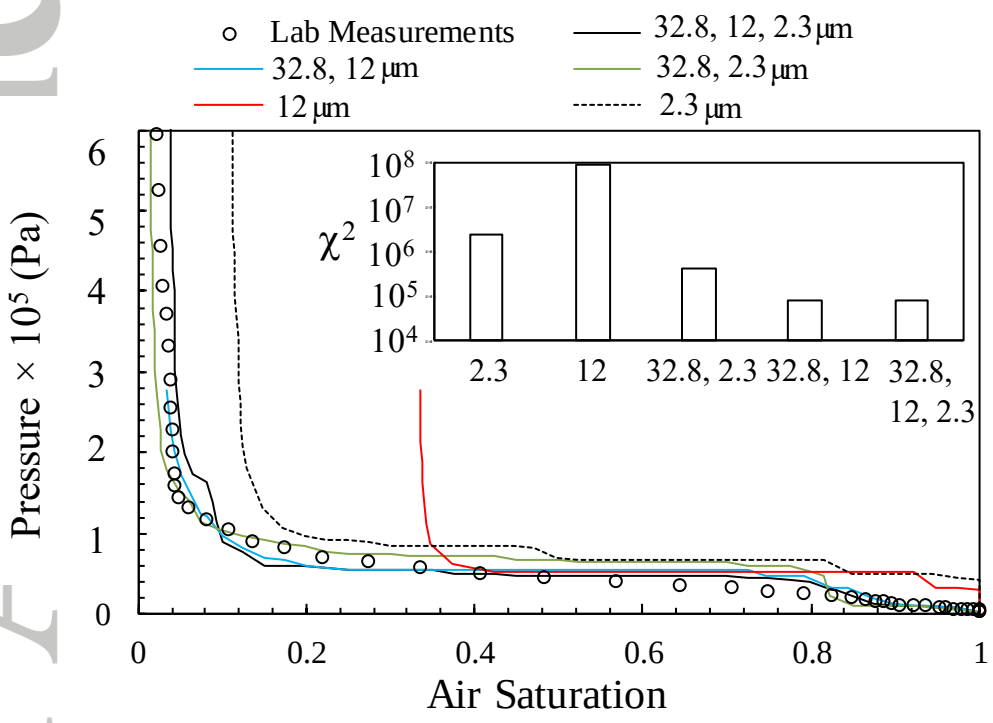

Figure 6. Figure